Undergrowth Collagen Fibers Analysis by Fingerprint Enhancement Method

Clara Manesco, Thierry Cloitre, Martà Martin-Fernandez, Yannick Gerber, Florence Perrin, Oscar Saavedra-Villanueva, Csilla Gergely

Biology of the Cell

Biology of the Cell

RESEARCH ARTICLE OPEN ACCESS

Undergrowth Collagen Fibers Analysis by Fingerprint Enhancement Method

Clara Manesco[1] | Thierry Cloitre[1] | Marta Martin[1] | Yannick Nicolas Gerber[2] | Florence Evelyne Perrin[1] | Oscar Saavedra-Villanueva[1] | Csilla Gergely[1]

[1]Laboratoire Charles Coulomb (L2C), Université de Montpellier, CNRS, Montpellier, France | [2]MMDN, Université de Montpellier, INSERM, Montpellier, France

Correspondence: Oscar Saavedra-Villanueva (oscar.saavedra-villanueva@inrae.fr) | Csilla Gergely (csilla.gergely@umontpellier.fr)

Received: 17 February 2025 | **Revised:** 17 February 2025 | **Accepted:** 4 March 2025

Funding: This study was funded by the ANR (the French National Research Agency) under the "Investissements d'avenir" program with the reference ANR-16-IDEX-0006.

Keywords: collagen | fibril characterization | image processing | second-harmonic generation (SHG) | segmentation

ABSTRACT

Collagen is a key protein in mammals that maintains structural integrity within tissues. A failure in fibrillar collagen reorganization can induce cancer or fibrosis formation, such as in spinal cord injury (SCI), where the healing process after the initial trauma leads to the formation of scar tissue, which includes fibrosis. As there is no current treatment targeting the fibrotic process directly, a better understanding of collagen properties can thus help to apprehend malignant states.

Characterization of collagen fibers has been widely explored on second-harmonic generation (SHG) images, due to the label-free nature of the SHG imaging technique. It has been performed with various fibers extraction methods such as curvelet transform (CT) implemented in the open-source software CurveAlign. However, when it comes to investigating undergrowth collagen fibers (collagen fibers that are still under reorganization) as observed in SCI, the CT method becomes complex to tune for nonadvanced users in order to properly segment the fibers. To improve collagen detection in the case of undergrowth fibers, we propose a methodology based on the fingerprint enhancement (FP-E) algorithm that requires fewer user input parameters and is less time-consuming. Our method was extensively tested on SHG data from injured spinal cord samples.

We obtained metrics that depicted changes in collagen organization over time, particularly a significant increase in fiber density, demonstrating the FP-E algorithm was properly adapted to address the evolution of collagen properties after SCI. Besides the simpler tuning of the method compared to commonly used software, the combination with further characterization of the extracted fibers could lead to consider fibrillar collagen as a biomarker in diseases where fibers are under development. The FP-E algorithm is provided in the article.

1 | Introduction

Collagen is the main structural and abundant protein in mammals. Collagen fibers are arranged in a specific pattern within tissues, such as the skin, tendons, and ligaments, to provide the necessary strength and flexibility for maintaining structural integrity. However, collagen can be reorganized in response to various stimuli, including injury, disease, or aging. Studies have shown that collagen reorganization is associated with some pathologies such as an increased risk of breast cancer. These studies have specifically found that changes in the structure of collagen fibers can create a micro-environment that promotes

Oscar Saavedra-Villanueva and Csilla Gergelya contributed equally.

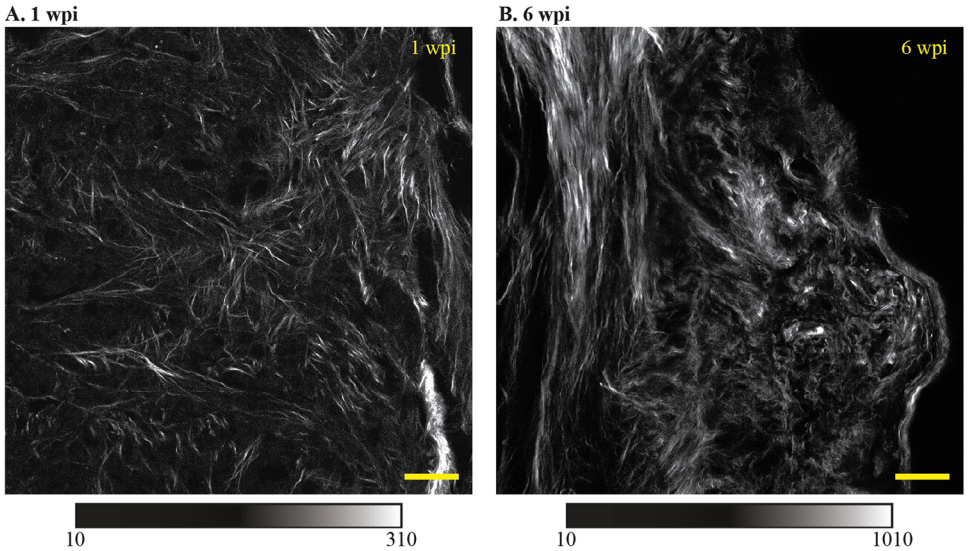

Figure 1 | Representative second-harmonic generation (SHG) images of collagen fibers undergrowth at the spinal cord injury area at different time points after lesion. (A) 1 wpi, (B) 6 wpi. An increment of fibers and bundle formation is observed over time. The scale bars are 50 μm. The corresponding lookup table (LUT) is displayed for each image.

tumor growth and invasion (Provenzano et al. 2006). The latter is because such altered collagen fibers can affect the behavior of cells within the tissue, including cancer cells. Collagen reorganization has also been found in nervous central system injuries and diseases such as in spinal cord injury (SCI). In this case, after injury, the axonal regeneration is partly inhibited by the glial scar, acting as a physical and chemical barrier (Alizadeh et al. 2019). The scarring process involves microglia, astrocytes, and extracellular matrix components, namely collagen, constructing the fibrotic component of the scar (Li et al. 2021). Recently, we reported that the fibrillar collagen of the scar is changing over time after SCI (Manesco et al. 2023), increasing its density and extension as shown in Figure 1.

In order to image fibrillar collagen, second-harmonic generation (SHG) imaging has emerged as a valuable technique for studying collagen in various biological tissues due to its key advantages of being noninvasive and label-free (Bancelin et al. 2015). SHG imaging thus allows the monitoring of collagen fibers without the need for exogenous dyes that may alter the native state of collagen. It also offers high spatial resolution, in-depth imaging, and sensitivity to structural changes (Ranjit et al. 2015).

Once collagen undergrowth has been imaged by SHG microscopy, supplementary data treatments for fiber extraction and characterization are needed to extract relevant fiber metrics. One of the most reliable methods is the combination of two complementary open-source software called CurveAlign and CT-FIRE (Liu et al. 2017). The method requires manual image preprocessing and extensive manual tuning of several fitting parameters resulting in a time-consuming procedure when a large number of images are analyzed. Moreover, the method becomes problematic to use for cases when collagen is yet in a reorganization process such as in SCI, where collagen is absent in the healthy tissue, but fibers appear and assemble gradually after the lesion (Figure 1). In the present article, we describe a new methodology for extracting and analyzing collagen fibers under reorganization (undergrowth) in tissues. The method is faster and relies on fewer user-input parameters and was extensively tested on SHG data acquired in an SCI study (Manesco et al. 2023). The proposed data treatment is based on the fingerprint-enhancement method and aims to extract from a raw image a binary skeletonized map of the individual fibers (or fiber bundles). The obtained binary map is then prone to be exploited in order to extract relevant metrics to characterize fibers.

Overall, the FP-E methodology combined with further characterization of the segmented fibers at different locations in the tissue and different time points after the injury/pathology allowed us to quantify collagen that can be employed as a biomarker (Manesco et al. 2023; Meurer et al. 2020; Almici et al. 2023; Williams et al. 2022) and help to reveal the efficiency of clinical treatments targeting fibrillar collagen.

2 | Material

2.1 | Animals, Lesion Model, Cares, and Sample Preparation

2.1.1 | Ethics Approval

Experimental work with animals followed the European legislative, administrative, and statutory measures for animal experimentation (EU/Directive/2010/63 of the European Parliament and Council) and the ARRIVE guidelines. The study was approved by the local ethics committee (no 36), by the Veterinary Services Department of Hérault, and by the French Ministry of National Higher Education and Research (authorization no 34118).

2.1.2 | Animals – Mice

Our study concerned the same animals as those used in a previous report (Poulen et al. 2021). CX3CR1+/eGFP transgenic female

mice were used, expressing enhanced green fluorescent protein (eGFP), downstream of the CX3CR1 promoter. The promoter is expressed in resident CNS microglia and peripheral monocytes. Animals were maintained in a C57BL/6 background (The Jackson Laboratory, Bar Harbor, ME, USA) and placed in controlled conditions for hygrometry, temperature, and a cycle light/dark of 12 h. Only heterozygotes were used. SHG imaging acquisitions were conducted on three animals per time-point, with two to five sections for each animal.

2.1.3 | Spinal Cord Injury and Postoperative Care

The protocol has been described elsewhere (Poulen et al. 2021). Shortly, mice were anesthetized with 3%–4% isoflurane (Vetflurane, Virbac, France). Anesthesia was then maintained with a 1%–2% isoflurane mixed with 1 L/min oxygen flow rate during the surgery, and eye gel was applied to the cornea. The lesion model consisted in a lateral spinal cord hemisection (HS) at Thoracic 9 level (T9) performed with a micro knife (10315-12, Fine Science Tools [FST]). Monitoring of the mice was conducted for 1 h after surgery. To overcome sphincter disability induced by the lesion, bladders were emptied manually twice a day until the full recovery of the sphincter control. Body weights were monitored before surgery, and then regularly until the end of the protocol. The current study presents analyses at 1 week postinjury (wpi) and 6 wpi.

2.1.4 | Histology and Sample Preparation

Animals received an intraperitoneal injection of tribromoethanol at a lethal dose (500 mg/kg, Sigma–Aldrich Darmstadt, Germany). They were perfused intracardially with PBS followed by paraformaldehyde (PFA) 4% (Sigma–Aldrich). The samples were postfixed in the same fixative then immersed in sucrose, embedded in Tissue-Tek O.C.T Compound, and frozen at −80°C. Serial 22 and 30 µm thick longitudinal spinal cord cryosections (Microm HM550, Thermofisher Scientific, Waltham, USA) were collected on Superfrost Plus slides using a cryostat (Microm HM550, Thermofisher Scientific, Waltham, MA, USA).

2.2 | Raw SHG Image

SHG images were acquired with a home-made multiphoton microscope (MPM) based on an upright SliceScope microscope (MPSS-1000P, Scientifica) equipped with a galvanometer scan head and a Nikon 16 × 0.8-NA water immersion objective (CFI75 LWD-16x-W). The samples were excited at 870 nm by a femtosecond Ti:Sapphire laser with ∼100 fs pulse duration at 80 MHz (Tsunami, Spectra Physics). The circular polarization of the beam was controlled by a combination of achromatic air-spaced half-wave and quarter-wave plates (EKS-467-4210 and EKS-467-4410, respectively, EKSMA Optics, Vilnius, Lithuania) mounted on rotary stages. The SHG signal was detected in transmission through a 1.4-NA water-immersion condenser (U-AAC, Olympus), filtered by a 482 nm long pass dichroic mirror (86-331, Edmund Optics), a 550 nm short pass filter (84-708 Edmund Optics), and a 447 nm high-performance band-pass filter (NT 48-074, Edmund Optics). The SHG signal was detected by a high-sensitivity GaAsP photomultiplier (H7422P, Hamamatsu). Z-stack images were performed in a field of view of 432 × 432 µm, at 1024 × 1024 pixels, and 2 µm z-step.

We acquired six SHG images at each z-position to construct a combined image in order to increase the signal-to-noise ratio (SNR). Data processing starts by reading the metadata providing the number of planes, then the different z-position images are summed up obtaining the Z-stack of SHG images. The Z-stack is converted into a double-precision matrix to bypass the limitation of mathematical operations with lower bit resolutions. A raw SHG image of collagen fibers in a lesioned SC tissue is shown in Figure 3A.

2.3 | Data Analysis Methods

Several methods have been reported to extract collagen fiber properties in a tissue from SHG microscopy images at different scales. Polarized-resolved SHG (P-SHG) measurements allow the assessment of the supramolecular organization of collagen within tissues (Almici et al. 2023). It has been reported that using fibers morphology as a scoring (such as fibrosis-SHG index in [Gailhouste et al. 2010]) or performing fast-Fourier transform (FFT) reveals the geometrical orientation of the fibers (Cicchi et al. 2013). One of the most reliable and accurate methods used to quantify fibrillar collagen is the methodology combining CurveAlign and CT-FIRE (Liu et al. 2017), based on the curvelet transform (CT) (Ma and Plonka 2010), widely used due to its efficiency in denoising fibers' images (Candès and Guo 2002; Starck et al. 2002) and enhancing the contrast to identify the feature's borders (Starck et al. 2003). However, CT depends on many parameters that are not evident to tune properly, rendering the software based on it complex for nonadvanced users. Multiple parameters need to be optimized and tuned to segregate accurately the fibers from the acquired images. This aspect is illustrated in Figure 2, with the example of tuning two parameters (the background threshold and size of the searching box) on not contrasted images and autocontrasted images, underlying the fact that the preprocessing steps and the sensitivity of those thresholds are crucial for fibers detection in SC injured tissue at 1 wpi.

To improve the detection of collagen fibers and adapt it to our samples' variability, we propose a new method based on the fingerprint enhancement (FP-E) algorithm. Biological tissues are known to be highly scattering and of very diverse composition. SC tissue presents different levels of collagen fibers after the lesion, justifying the need for more accurate methods to detect them. FP-E is mainly used in forensic science to improve the quality and clarity of fingerprint images by extracting their ridges. The method is highly efficient in enhancing the ridge patterns and details of the fingerprint (Hong et al. 1998). It thus represents a promising method to extract collagen fibers.

2.3.1 | Fingerprint Enhancement Method

The algorithm for data processing and analysis was constructed under MATLAB 2021a. The pipeline of the method is summarized in Figure 3. After the image acquisitions, the sequence of the data analysis includes different steps to obtain a final skeleton map

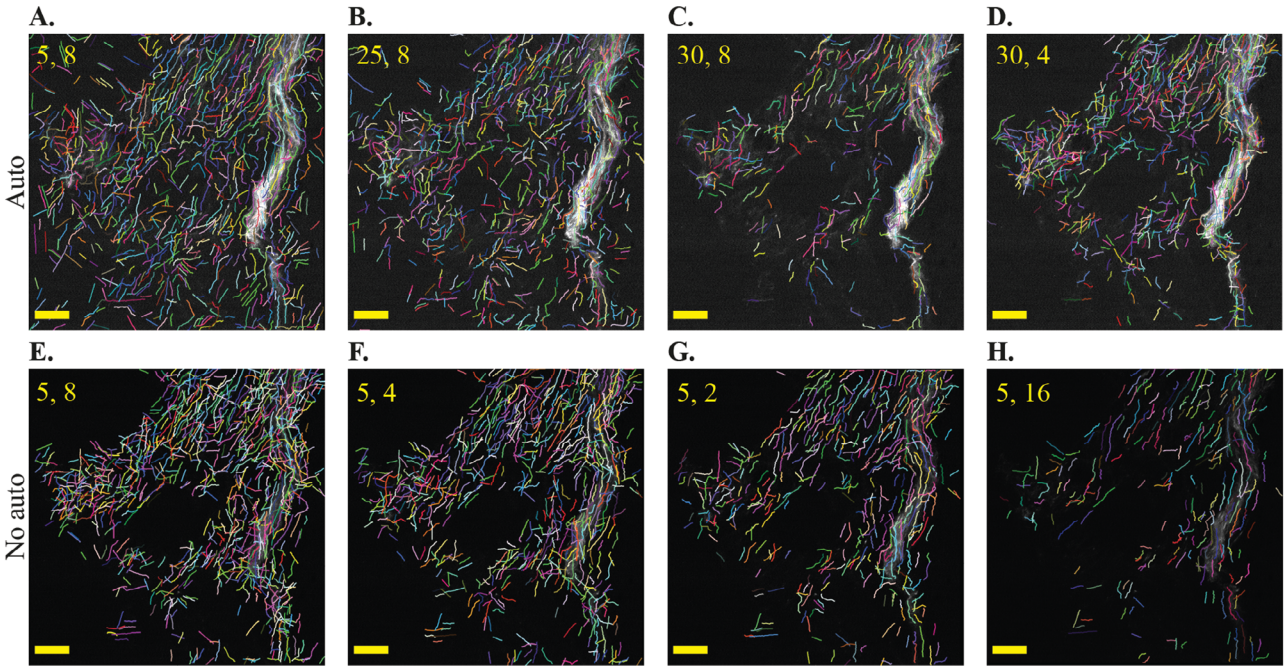

Figure 2 | Example of the influence of different input parameters in the CurveAlign method for the segmentation of collagen fibers in injured SC tissue at 1 wpi. The background threshold (first number) and the size of the searching box in pixels (second number) were tested on second-harmonic generation (SHG) images with and without autocontrasting, top and bottom images, respectively. No background subtraction was applied. The default values are set to 5 and 8 for the background threshold and the box size, respectively. Increasing the background threshold decreases the number of fibers detected while decreasing the box size increases the detection. Scale bars are 50 μm.

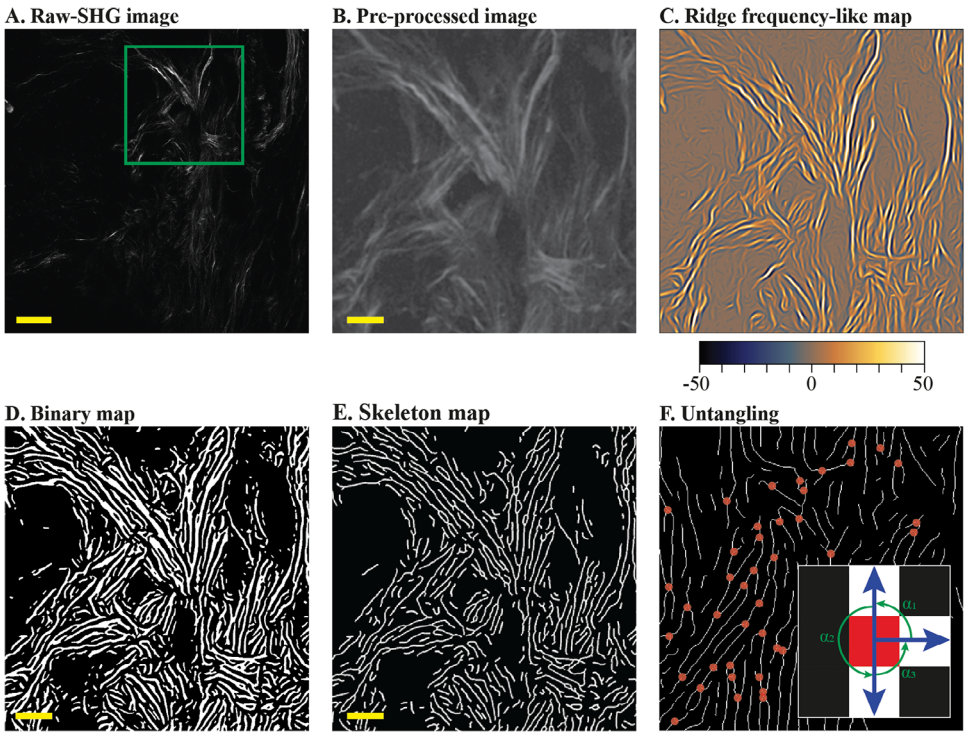

Figure 3 | Pipeline of the Fingerprint enhancement-based method. (A) Raw second-harmonic generation (SHG) image (scale-bar is 50 μm). The green frame shows the zoom-in displayed in the following images. (B) Preprocessed image applying signal enhancements and oversampling (scale-bar is 20 μm). (C) Ridge frequency-like map obtained by fingerprint enhancement method. (D) Binary map of fibers determined by all positive values in (C). (E) Skeleton maps of fibers obtained from the binary map in (D). (F) Untangling of fibers by geometrical constraints applied on the skeleton map.

from the preprocessed images that is then exploited to obtain the metrics for fibers characterization. The image treatment includes computing a reliability map, a ridge frequency-like image, and a binary mask from a threshold version of the reliability map. This binary mask is subsequently applied to a binarized version of the frequency-like map to provide a binary image. Finally, this binary image is skeletonized, the fibers are untangled, and the fibers map is obtained. The details of each image treatment step are given below.

A. Preprocessing: The image preprocessing begins by enhancing the contrast of each single plane of the Z-stack SHG image with a Rayleigh distribution shape, followed by a Gaussian filter to decrease the image noise. Then, an image resizing (oversampling) is performed to increase the image size and so the number of pixels where the fiber's border can be defined. In our data analysis, the scale factor was set at 2, allowing better detection of the fibers by increasing the space where their border can be defined. The chosen oversampling factor of two is an optimal compromise between the computational cost and the efficiency of the following steps to extract the fibers. The output of this preprocessing is shown in Figure 3B.

B. Fiber skeleton map extraction: In order to identify the collagen fibers, ridge-like regions (regions with a high chance of finding a collagen fiber) are determined by evaluating the standard deviation of the signal intensity in a moving window of 8 × 8 pixels across the preprocessed image (for simplicity for future users of the FP-E algorithm, we will call it "fingerprint threshold"). When the standard deviation in the evaluated window is above a defined threshold (depending mainly on the image SNR), it is deemed part of a ridge. In Figure 4, using a typical example, we highlight how different threshold values can affect the quantity of fibers detected across the tissue. We have found that in most cases this value ranked between 0.02 and 0.30 with a typical value of 0.04. In our method, the fingerprint threshold is the only parameter to be tuned manually within a reduced and defined range, presenting a great advantage in terms of saving computing time for the user.

Once the ridge-like regions are evaluated, the local ridge orientation axis needs to be estimated by calculating the area moment of the preprocessed image at each point. It is done by determining the principal axis of the intensity variation (gradients) as follows (Hong et al. 1998, Kovesi)

$$\nabla I_{\mathrm{SHG}}(x,y) = \begin{bmatrix} G_x & G_y \end{bmatrix} = \begin{bmatrix} \frac{\partial I_{\mathrm{SHG}}}{\partial x} & \frac{\partial I_{\mathrm{SHG}}}{\partial y} \end{bmatrix}$$

where $I_{\mathrm{SHG}}(x,y)$ is the SHG intensity signal in the (x,y) position, G_x and G_y are the partial derivatives of the intensity to x and y, respectively. The elements of the covariance matrix are then determined for the image gradient as:

$$G_{xx} = G_x^2$$
$$G_{xy} = G_x \cdot G_y$$
$$G_{yy} = G_y^2$$

The covariance matrix is then diagonalized to determine its principal directions. The analytic solution of the principal direction of the covariance matrix is given by:

$$G'_{\min} = \frac{G_{yy} + G_{xx}}{2} - \frac{(G_{xx} - G_{yy})}{2} \cdot \cos(2\gamma) - \frac{G_{xy}}{2} \cdot \sin(2\gamma)$$

$$G'_{\max} = G_{yy} + G_{xx} - G'_{\min}$$

where $G'_{\max}$ is the principal axis of the covariance (and the maximum area moment), $G'_{\min}$ is the minimum area moment, and γ is the rotation angle applied to diagonalize the matrix, which can be determined as follows:

$$\sin(2\gamma) = \frac{G_{xy}}{\sqrt{G_{xy}^2 + (G_{xx} - G_{yy})^2}}$$

$$\cos(2\gamma) = \frac{G_{xx} - G_{yy}}{\sqrt{G_{xy}^2 + (G_{xx} - G_{yy})^2}}$$

Then, a reliability map can be obtained as follows:

$$\text{reliability} = 1 - \frac{G'_{\min}}{G'_{\max}}$$

The reliability value obtained for each pixel is in the [0, 1] range, with 1 representing a fully reliable value. The reliability value reflects the local anisotropy of the SHG intensity variation rate and is therefore a good estimator to detect highly anisotropic objects such as elongated fibers.

Sequentially, a ridge frequency-like map (Figure 3C) was obtained according to Hong and colleagues (Hong et al. 1998). Briefly, this map shows the ridge spatial frequency (or modulation) obtained by estimating the local ridge orientation and frequency as previously explained. Then, the positive values of the ridge frequency-like map are set to 1 in order to determine the ridge-like image. Subsequently, the reliability map is multiplied by the ridge-like image, generating a binary map of the fibers (Figure 3D). From the binary map of the fibers, the central line of each feature is determined leading to a skeleton map (Figure 3E). Collagen fibers are highly densely distributed within the tissue as shown in Figures 1 and 3 thus the skeleton map contains many merged fibers. Therefore, we developed an untangling method (Figure 3F) based on the fibers geometrical constraints applied to the skeleton map. The branch points were found and a subimage of a 1-pixel radius around each branch point was analyzed to evaluate the fiber continuity. The most reasonable fiber continuity was determined by identifying each possible connection's angle (α) around the branch point (Figure 3F). Once the skeleton map has been untangled, different metrics are computed to characterize the fibrils. The relevant metrics were assessed from the skeletonized map of the collagen fibers.

C. Defined metrics: The parameters deduced were the fibers' density (defined as the total length of the fibers divided by the tissue area in the image), tortuosity, local alignment map of the fibers, and the statistical entropy as defined in our previous study (Manesco et al. 2023), briefly recalled here:

- Fibers' total length: the sum of all the fibers' skeleton lengths measured across the whole image.

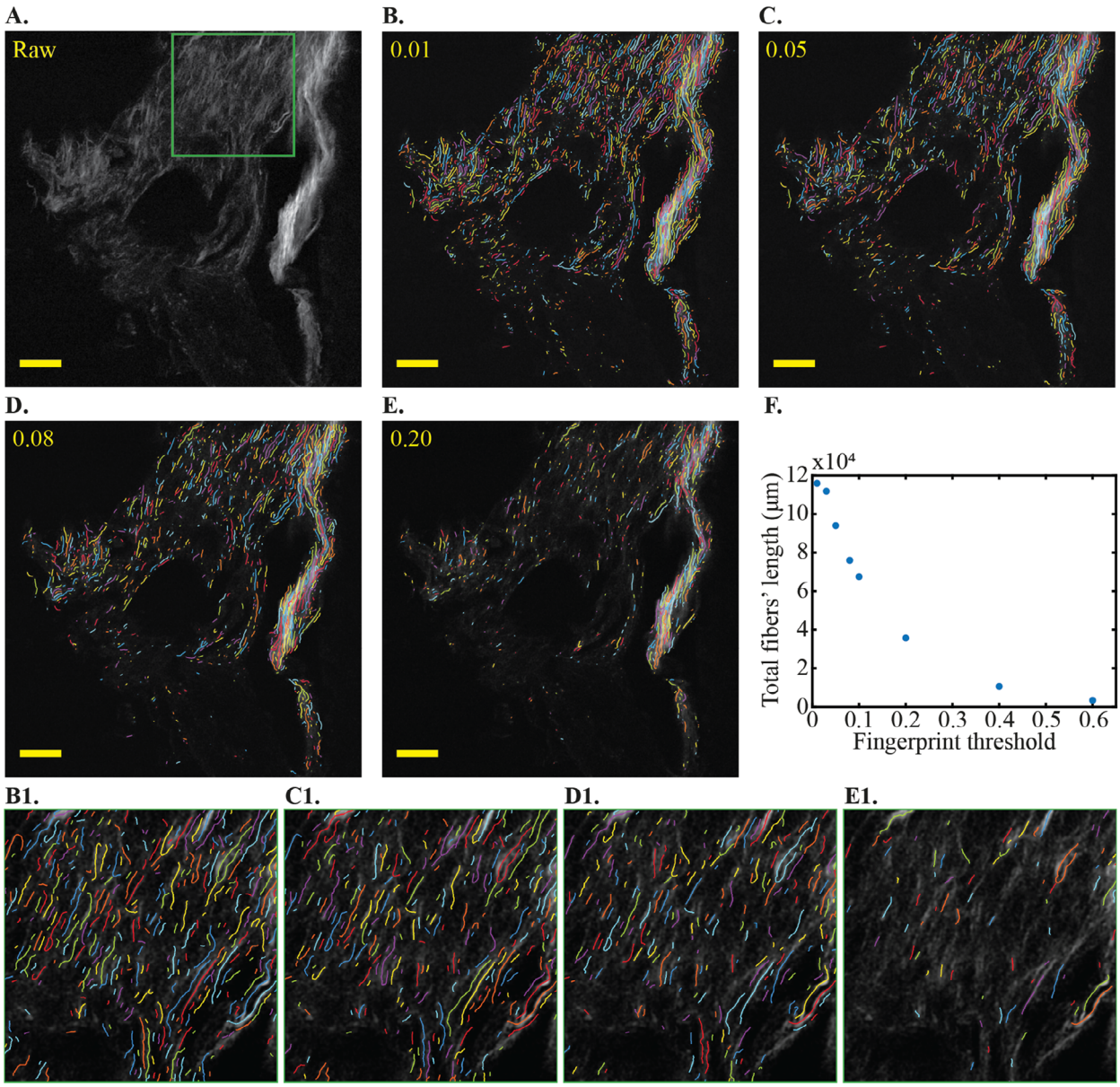

Figure 4 | The performance of the fingerprint method at various input parameters. (A) The raw second-harmonic generation (SHG) image. Fingerprint threshold tuned as (B) 0.01, (C) 0.05, (D) 0.08, (E) 0.20. The zoomed ROI in (A) for the different fingerprint thresholds are presented in (B1), (C1), (D1), and (E1). (F) Graph showing that the detected total fibers' length decreases when the fingerprint threshold rises. Scale bars are 50 µm.

- Fibers' density (φ): the quantity of fibers detected across the tissue surface occupied in the image.

$$\phi = \frac{F_l}{S_t}$$

with F_l the sum of the fiber's length detected across the tissue and S_t the tissue area.

- Tortuosity: used to quantify the straightness of individual fibers. The tortuosity is computed as the fiber length ratio over the fiber end-to-end distance (Shanti et al. 2014). The lowest the tortuosity, the straighter the fiber.

- Statistical entropy (S): quantifying the global fibers' organization within the tissue by evaluating the orientation distribution at the pixel level computed from the skeleton map following Ducourthial et al. (2019):

$$S = \frac{-1}{\mathrm{Ln}\,(\mathrm{NB})} \sum_{\beta=-90°}^{90°} p\,(\beta)\,\mathrm{Ln}\,(p\,(\beta))$$

where NB is the number of bins, β is the angular bin used, and $p(\beta)$ is the normalized number of pixels with the orientation β in the local orientation map as explained in (Manesco et al. 2023). The statistical entropy provides the degree of orientation disorder at the tissue level: $S = 1$ means a fully isotropic orientation distribution, whereas smaller S values suggest a narrower distribution of the orientation.

- Variance: the local alignment of fibers assessed by computing the circular statistical variance for different local orientations

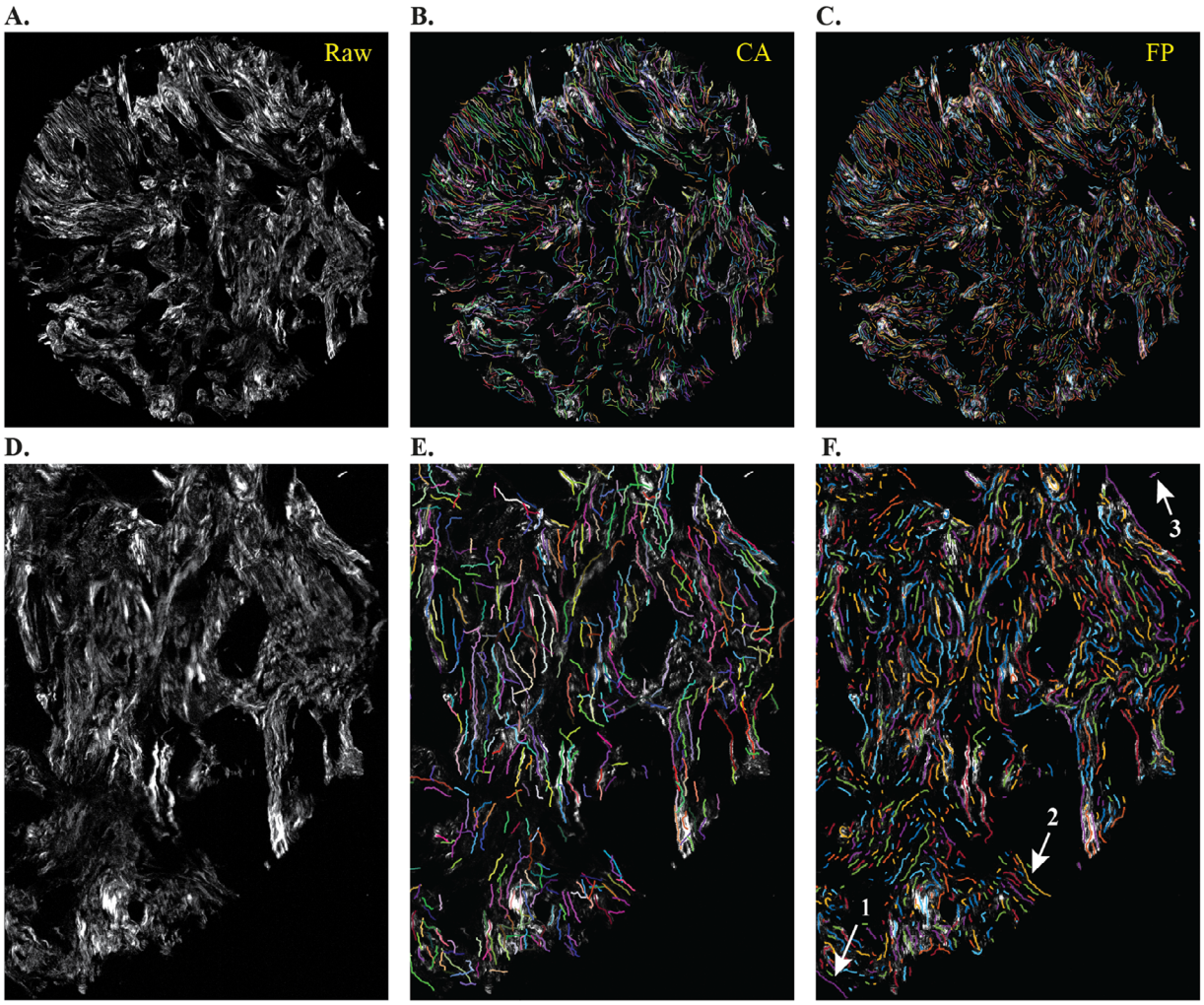

Figure 5 | Comparison of collagen fibers' detection by CurveAlign and Fingerprint methods. (A) Raw second-harmonic generation (SHG) image of breast cancer tissue is analyzed by both methods, (B) CurveAlign, and (C) Fingerprint method. A zoom-in of each top image is shown in (D), (E), and (F). White arrows highlight the observed differences in both methods. The fingerprint method found a total fibers' length of 80.5×10^3 pixels, whereas the CurveAlign method detected 49.3×10^3 pixels.

with $\theta \in [-90°, 90°)$. The circular variance is evaluated as follows (Mardia and Jupp 1999):

$$\mathrm{Var}(\theta) = \frac{1}{N}\sum_{j=1}^{N}\left(1 - \cos\left(2\theta_j - 2\bar{\theta}\right)\right)$$

where θ_j is the orientation of a pixel associated with a skeleton fiber and $\bar{\theta}$ is the mean orientation computed as follows:

$$\bar{\theta} = \frac{\arg\left\{\sum_{j=1}^{N} e^{i2\theta_j}\right\}}{2}$$

with $\mathrm{Var}(\theta) = 0$ for perfectly aligned fibers, and $\mathrm{Var}(\theta) = 1$ for randomly oriented fibers. The method to obtain the local alignment map is described in detail in our previous work (Manesco et al. 2023).

2.4 | Statistics

Repeated measurements and the mixed effect model were necessary as the compared samples were paired and not always of the same size. A paired *t* test with Welch's correction was used for comparing the computed metrics for 1 and 6 wpi. Tukey's multiple comparisons were employed after performing normality tests for comparison of every mean with every other mean. Three mice were analyzed for each condition; each dot represents an acquisition area in the plots. Statistical significance was set at $p \leq 0.05$.

3 | Results and Discussion

The purpose of using the FP-E method was to ease the analysis of undergrowth collagen fibers within injured spinal cord tissues in a murine model. As illustrated in Figure 1, the collagen fibers did not only evolve in terms of organization over time but also in terms of fibers' growth: the SHG image at 1wpi showed an apparent weaker signal compared to the image at 6 wpi, where the signal was enhanced with fibers growing in a completely different orientation pattern.

These changes were first apprehended with CurveAlign, assessing the number, the length, and the orientation of the fibers,

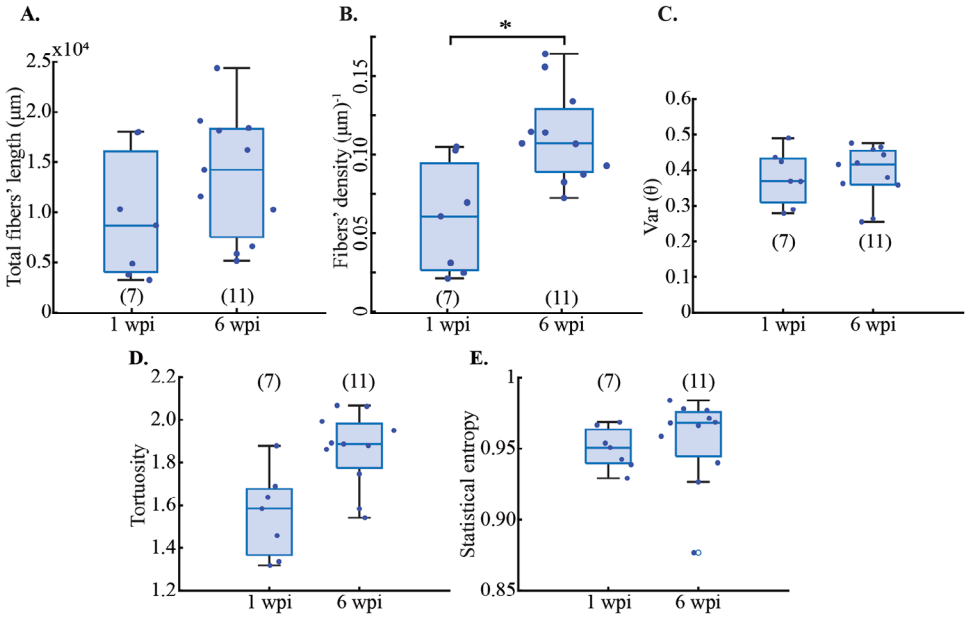

Figure 6 | Spinal cord injury metrics extracted by the fingerprint method at two time points: 1 and 6 wpi. (A) Total fibers' lengths across the tissue. (B) Fibers' density across the tissue. (C) Relative orientation (variance) within a radius of 40 μm. (D) Tortuosity of fibers. (E) Statistical entropy, a larger dispersion of entropy is noticed over time. With $*p < 0.05$. 3 mice were analyzed per time point. The number of samples analyzed is shown into brackets.

but no significant statistical differences were found over time for all the investigated metrics, despite they seem different in the SHG images at 1 and 6 wpi (Manesco 2023). This suggests that some information is lost during data analysis. That may be partially due to the fact that tuning the software thresholds is not straightforward, as depicted in Figure 2. In this example, two parameters were tuned, the background threshold and the size box (these two parameters have been reported to affect the fibers detection – see CurveAlign FAQ). Changing these threshold values greatly impacted the fibers definition, and it was difficult to define the best thresholds for optimal fibers detection according to the input image. The same image was then investigated with the FP-E method, evidencing the impact of changing only one parameter, in our case the Fingerprint threshold by quantifying the total fibers length. The effect of the tuning is illustrated in Figure 4, showing a decrease in total fibers length when the Fingerprint threshold rises. The tuning-metric dependency could thus be easily monitored with this approach.

A more global comparison between the two methods was carried out on collagen fibers observed in breast cancer tissue and is presented in Figure 5. It is important to note that this image analysis using CurveAlign (Figure 5B, E) was carried out by their developers and published with the code on their software website (https://github.com/uw-loci/curvelets/releases/download/5.0/CA5.0andCTF3.0_manual_testImages.zip). Whereas the FP-E analysis conducted on the same image was performed by us, the developers of the FP-E method. This comparison highlighted apparent similar results for many areas; however, a more in-depth analysis shows more fibers detected with the FP-E method. This can be explained by the untangling method step that segments the fibers instead of keeping them merged, so more short fibers are expected. Some areas, indicated by white arrows, highlight some specific differences: a missed detection (Arrow 1), where a fragment is not detected by CA while considered as a fiber by FP-E, the segmentation difference (Arrow 2), where CA detected two fibers while FP-E revealed a single fiber, and the angle consideration (Arrow 3), where CA identified two fibers almost at 90°, while FP-E together with the untangling method defined the most probable angle for the final detection. The differences provided by the two methods can be quantified by computing the total fibers' length detected by both. The fingerprint method found a total fibers' length of 80.5×10^3 pixels, whereas the CurveAlign method detected 49.3×10^3 pixels. In both cases, the threshold needed to be adapted for a proper comparison of the images containing complicated data to analyze, and at this point, no method can be regarded as better than the other.

Several studies also compared CurveAlign with other alternative fibers detection methods. A comparison with an adapted Fingerprint algorithm has been reported when assessing collagen characterization in gels (Sun et al. 2015). This comparison showed an overall similar accuracy in the detected fibers, yet pointing out a faster calculation time in the fingerprint method (CPU time = 0.730 s) compared to CA (CPU time = 1.680 s) when both methods are executed in the same computer. Methods dedicated to collagen fibers detection have also been used as complementary tools (Despotović et al. 2020), involving various specialized software (CT-FIRE, CurveAlign, and FiberFit) to characterize the collagen fibers in colon cancer. Each method was specifically dedicated to a particular assessment: CT-FIRE was to evaluate the straightness and width, CurveAlign to define the alignment, and FiberFit to characterize the defined alignment. In De Vries et al. (2023) review, the authors provided recommendations to choose the adapted methods for fibers' assessment. For example, CurveAlign and FiberFit were chosen to study the fibers alignment, while total fibers' length was determined using another method, conceived by Fricker et al., and initially dedicated to extract the morphology of endoplasmic reticulum in plants (Fricker et al. 2018).

In our case, detection of collagen fibers by the FP-E enabled us to compute several metrics revealing changes over time, as presented in Figure 6. Both total fibers' length (13.6±6.3 mm at 6 wpi and 9.6±6.3 mm at 1 wpi) and fibers' density ($0.13 \pm 0.02\ \mu m^{-1}$ at 6 wpi and $0.06 \pm 0.03\ \mu m^{-1}$ at 1 wpi) showed higher values at 6 wpi compared to 1 wpi, with a significant statistical difference for the fibers' density ($p = 0.282$), indicating an increase in collagen fibers formation at 6 wpi. This observation agrees with the qualitative observation of fibers in Figure 1 and was investigated in depth in another work (Manesco et al. 2023). Also, fibers were found to become less straight over time, since the tortuosity increased at 6 wpi (1.9 ± 0.2), compared to 1 wpi (1.6 ± 0.2). The relative orientation expressed by the variance showed low and similar values for both time points (0.38 ± 0.08 at 1 wpi and 0.39 ± 0.08), suggesting that fibers are rather well aligned with each other and no reorientation was detected over time. Statistical entropy was globally high (between 0.90 and 0.95) with a larger dispersion over time, suggesting a preferential orientation at 6 wpi at the tissue level.

4 | Conclusions

The main achievement when using the FP-E algorithm was the segmentation of undergrowth and dense collagen fibers from SHG images and their characterization. The obtained metrics using our method suggest changes over time with a significant statistical difference for the fiber's density between 1 and 6 wpi. This indicates that the fingerprint-enhanced method is sensitive enough to extract collagen fibers in excised spinal cord tissue.

In comparison with standard fibers segmentation methods, FP-E is easier to use, with a single parameter to tune the FP-threshold, while other methods such as the CT algorithm require more tuning and longer processing-time. The method is provided as an open-source code, considerably easing the access and updates. Also, our method works with 16-bit images as input data which contain more information than the 8-bit images required in CurveAlign. Consequently, the metrics we deduced to characterize the fibers are easy to implement and highly sensitive evidencing important modifications in collagen fibers organization after injury of the SC in a mice model.

Both the FP-E method and CT algorithm show good results for the fibers' identification, though our comparisons suggest that the FP-E is more suitable for detecting small fibers in their undergrowth phase. None of the methods can be considered better than the other in terms of segmentation, but the proposed FP-E method is based on a rather simple algorithm, where a single threshold needs to be tuned, it is therefore easier and faster, which makes it globally more user-friendly. A MATLAB implementation of the FP-E algorithm is available at https://github.com/users/OscarSaavedra-Villanueva.

Author Contributions

C.M. and O.S.V. performed the laboratory studies, the SHG experiments, the data analysis and wrote the original draft. O.S.V. developed the software. M.M. performed the statistical analysis. Y.N.G. and F.P. provided the biological and physiological expertise. C.M., T.C., M.M., O.S.V., and C.G. provided the expertise in physics and microscopy. F.P., C.G., and T.C. designed the study, supervised the investigations, and data interpretation. C.G. assured the funding acquisition, the project administration, and its validation. All authors provided critical review of the manuscript and approved its submission.

Acknowledgments

The authors thank the ANR (the French National Research Agency) under the "Investissements d'avenir" program with the reference ANR-16-IDEX-0006 for the support.

Conflicts of Interest

The authors declare no conflicts of interest.

Data Availability Statement

The data that support the findings of this study are available from the corresponding author upon reasonable request.

References

Alizadeh, A., S. M. Dyck, and S. Karimi-Abdolrezaee. 2019. "Traumatic Spinal Cord Injury: An Overview of Pathophysiology, Models and Acute Injury Mechanisms." *Frontiers in Neurology* 10: 282. https://doi.org/10.3389/fneur.2019.00282.

Almici, E., M. Arshakyan, J. L. Carrasco, et al. 2023. "Quantitative Image Analysis of Fibrillar Collagens Reveals Novel Diagnostic and Prognostic Biomarkers and Histotype-Dependent Aberrant Mechanobiology in Lung Cancer." *Modern Pathology* 36: 100155. https://doi.org/10.1016/j.modpat.2023.100155.

Bancelin, S., B. Lynch, C. Bonod-Bidaud, et al. 2015. "Ex Vivo Multiscale Quantitation of Skin Biomechanics in Wild-Type and Genetically-Modified Mice Using Multiphoton Microscopy." *Scientific Reports* 5: 17635. https://doi.org/10.1038/srep17635.

Candès, E. J., and F. Guo. 2002. "New Multiscale Transforms, Minimum Total Variation Synthesis: Applications to Edge-Preserving Image Reconstruction." *Signal Processing* 82: 1519–1543. https://doi.org/10.1016/S0165-1684(02)00300-6.

Cicchi, R., N. Vogler, D. Kapsokalyvas, B. Dietzek, J. Popp, and F. S. Pavone. 2013. "From Molecular Structure to Tissue Architecture: Collagen Organization Probed by SHG Microscopy." *Journal of Biophotonics* 6: 129–142. https://doi.org/10.1002/jbio.201200092.

Despotović, S. Z., Đ. N. Milićević, A. J. Krmpot, et al. 2020. "Altered Organization of Collagen Fibers in the Uninvolved Human Colon Mucosa 10 cm and 20 cm Away From the Malignant Tumor." *Scientific Reports* 10: 6359. https://doi.org/10.1038/s41598-020-63368-y.

De Vries, J. J., D. M. Laan, F. Frey, G. H. Koenderink, and M. P. M. De Maat. 2023. "A Systematic Review and Comparison of Automated Tools for Quantification of Fibrous Networks." *Acta Biomaterialia* 157: 263–274. https://doi.org/10.1016/j.actbio.2022.12.009.

Ducourthial, G., J. S. Affagard, M. Schmeltz, et al. 2019. "Monitoring Dynamic Collagen Reorganization During Skin Stretching With Fast Polarization-Resolved Second Harmonic Generation Imaging." *Journal of Biophotonics* 12: e201800336. https://doi.org/10.1002/jbio.201800336.

Fricker, M., L. Heaton, N. Jones, B. Obara, S. J. Müller, and A. J. Meyer. 2018. "Quantitation of ER Structure and Function." *Methods in Molecular Biology* 1691: 43–66.

Gailhouste, L., Y. L. Grand, C. Odin, et al. 2010. "Fibrillar Collagen Scoring by Second Harmonic Microscopy: A New Tool in the Assessment of Liver Fibrosis." *Journal of Hepatology* 52: 398–406. https://doi.org/10.1016/j.jhep.2009.12.009.

Hong, L., Y. Wan, and A. K. Jain. 1998. "Fingerprint Image Enhancement: Algorithm and Performance Evaluation." *IEEE Transactions on Pattern*

Analysis and Machine Intelligence 20: 777–789. https://doi.org/10.1109/34.709565.

Kovesi, P. "MATLAB and Octave Functions for Computer Vision and Image Processing." Peter's Functions for Computer Vision. Accessed February 17, 2025. https://www.peterkovesi.com/matlabfns/index.html.

Li, Z., S. Yu, X. Hu, et al. 2021. "Fibrotic Scar After Spinal Cord Injury: Crosstalk With Other Cells, Cellular Origin, Function, and Mechanism." *Frontiers in Cellular Neuroscience* 15: 720938. https://doi.org/10.3389/fncel.2021.720938.

Liu, Y., A. Keikhosravi, G. S. Mehta, C. R. Drifka, and K. W. Eliceiri. 2017. "Methods for Quantifying Fibrillar Collagen Alignment." *Methods in Molecular Biology* 1627: 429–451.

Ma, J., and G. Plonka. 2010. "The Curvelet Transform." *IEEE Signal Processing Magazine* 27: 118–133. https://doi.org/10.1109/MSP.2009.935453.

Manesco, C. 2023. "Photonic and Nanomechanical Study for Label-Free Monitoring of the Fibrotic Scar in Spinal Cord Injury in Mice." (Doctoral dissertation, Université de Montpellier) English. NNT: 2023UMONS072.

Manesco, C., O. Saavedra-Villanueva, M. Martin, et al. 2023. "Organization of Collagen Fibers and Tissue Hardening: Markers of Fibrotic Scarring After Spinal Cord Injury in Mice Revealed by Multiphoton-Atomic Force Microscopy Imaging." *Nanomedicine: Nanotechnology, Biology and Medicine* 53: 102699. https://doi.org/10.1016/j.nano.2023.102699.

Mardia, K. V., and P. E. Jupp eds. 1999. *Directional Statistics*. John Wiley & Sons, Inc.

Meurer, S. K., M. A. Karsdal, and R. Weiskirchen. 2020. "Advances in the Clinical Use of Collagen as Biomarker of Liver Fibrosis." *Expert Review of Molecular Diagnostics* 20: 947–969. https://doi.org/10.1080/14737159.2020.1814746.

Poulen, G., E. Aloy, C. M. Bringuier, et al. 2021. "Inhibiting Microglia Proliferation After Spinal Cord Injury Improves Recovery in Mice and Nonhuman Primates." *Theranostics* 11: 8640–8659. https://doi.org/10.7150/thno.61833.

Provenzano, P. P., K. W. Eliceiri, J. M. Campbell, D. R. Inman, J. G. White, and P. J. Keely. 2006. "Collagen Reorganization at the Tumor-Stromal Interface Facilitates Local Invasion." *BMC Medicine* 4: 38. https://doi.org/10.1186/1741-7015-4-38.

Ranjit, S., A. Dvornikov, M. Stakic, et al. 2015. "Imaging Fibrosis and Separating Collagens Using Second Harmonic Generation and Phasor Approach to Fluorescence Lifetime Imaging." *Scientific Reports* 5: 13378. https://doi.org/10.1038/srep13378.

Shanti, N. O., V. W. L. Chan, S. R. Stock, F. De Carlo, K. Thornton, and K. T. Faber. 2014. "X-Ray Micro-Computed Tomography and Tortuosity Calculations of Percolating Pore Networks." *Acta Materialia* 71: 126–135. https://doi.org/10.1016/j.actamat.2014.03.003.

Starck, J.-L., E. J. Candès, and D. L. Donoho. 2002. "The Curvelet Transform for Image Denoising." *IEEE Transactions on Image Processing* 11: 670–684. https://doi.org/10.1109/TIP.2002.1014998.

Starck, J.-L., F. Murtagh, E. J. Candes, and D. L. Donoho. 2003. "Gray and Color Image Contrast Enhancement by the Curvelet Transform." *IEEE Transactions on Image Processing* 12: 706–717. https://doi.org/10.1109/TIP.2003.813140.

Sun, M., A. B. Bloom, and M. H. Zaman. 2015. "Rapid Quantification of 3D Collagen Fiber Alignment and Fiber Intersection Correlations With High Sensitivity." *PLoS ONE* 10: e0131814. https://doi.org/10.1371/journal.pone.0131814.

Williams, L., T. Layton, N. Yang, M. Feldmann, and J. Nanchahal. 2022. "Collagen VI as a Driver and Disease Biomarker in Human Fibrosis." *The FEBS Journal* 289: 3603–3629. https://doi.org/10.1111/febs.16039.